Pergamon

Int. J. Heat Mass Transfer. Vol. 41, No. 2, pp. 425–433, 1998

Printed in Great Britain
0017–9310/98 $19.00 + 0.00

PII: S0017–9310(97)00112–9

Effect of the leakage on pressure drop and local heat transfer in shell-and-tube heat exchangers for staggered tube arrangement

HUADONG LI and VOLKER KOTTKE

Institute of Food Technology, Department of Food Process Engineering, Hohenheim University, 70599 Stuttgart, Germany

(*Received* 18 *November* 1996 *and in final form* 11 *March* 1997)

Abstract—Experiments are performed to determine the response of the pressure drop and local heat transfer on the shell side of shell-and-tube heat exchangers to a change in the leakage between baffles and shell in the fully developed regime. The local mass and heat transfer coefficients are visualized and determined by means of mass transfer measurements. The shell-side flow distribution was calculated from the measurements of the pressure distribution in the baffle compartment. This leakage between baffles and shell can greatly reduce the pressure drop and the per-compartment average heat transfer coefficient.

INTRODUCTION

The optimization of shell-and-tube heat exchangers requires a good knowledge of the local and average shell-side heat transfer coefficients. Heat transfer in the baffled cylindrical shell-side is complicated by a number of geometrical factors: shell diameter, baffle cut, baffle spacing, tube diameter, pitch, arrangement and clearances or leakage paths. Clearances, which are required for mechanical assembly reasons, allow leakage streams between the baffles and the shell and between the baffles and the tubes. These leakages reduce the velocity in the tube bundle and, hence, the heat transfer coefficient and pressure drop.

A great deal of experimental and analytical studies have been devoted to the effect of the leakages on the pressure drop and the integral heat transfer coefficient [1–4]. Recently, several models have been applied to analyze flow and thermal transfer [5–7], but these models can only provide the integral heat transfer coefficient.

In this paper, experiments have been performed to determine the response of pressure drop and local heat transfer on the shell side of shell-and-tube heat exchangers to a change in the leakage between baffles and shell in the fully-developed regime by using a mass transfer technique based on absorption, chemical and coupled colour reaction [8–10]. In order to get the shell-side flow distribution, the pressure distribution in a baffle compartment is measured. In addition, the detailed local distribution of the heat transfer coefficient in the baffle-tube clearances will also be presented.

EXPERIMENTS

The shell-and-tube heat exchanger used in this work is shown in Fig. 1(a). It consists of (1) a cylindrical plexiglass shell and (2) two removable PVC tube sheets, which support (3) a bundle of glass tubes and (4) eight tie rods. The test section is located in the third baffle-compartment, which is in the fully-developed flow region, from the exchanger inlet. The shell-baffle leakage can be eliminated by plastic sealings. Figure 1(b) shows the internal configuration of the heat exchanger. Because of the symmetric tube arrangement, only 20 tubes are presented. Each tube location is denoted by two numbers, the first of these is the number of the row from top to bottom, where the tube is located. The second number from left to right indicates the tube position within the row. The eight tie rods can greatly reduce the by-passing between bundle and shell. All of the tubes were made removable and can be replaced by a pressure sensing tube [Fig. 1(c)] or by a mass transfer measuring tube [Fig. 1(d)]. The main dimensions and features of the heat exchangers are given in Table 1.

For the visualization and mass transfer measurements, a mass transfer technique based on absorption, chemical and coupled colour reaction [8–11] is used. The surface of the mass transfer measuring tube is coated with a wet filter paper containing an aqueous solution of manganese(II)chloride with hydrogenperoxide, and is inserted in the heat exchanger. Air is sucked in by a suction fan. The reaction gas (ammonia) is added as a pulse to the main stream in very low concentration. Because of its distinguished

NOMENCLATURE

a	pitch ratio
A	flow area $A = D_i S$ [m^2]
C_p	specific heat capacity [KJ (kg K)$^{-1}$]
d	tube outside diameter [m]
D	diameter of baffle hole [m]
D_i	inside diameter of the shell [m]
l	characteristical length $l = \pi d/2$ [m]
L	distance of two baffle compartments [m]
Nu	Nusselt number $Nu = \alpha d/\lambda$
ΔP_1	pressure drop in two compartments [N m^{-2}]
ΔP_2	pressure drop in clearance [N m^{-2}]
Re	Reynolds number $Re = u1/(\psi v)$
Re_{eff}	effective Reynolds number
S	baffle spacing [m]
u	fluid velocity $u = \dot{V}/A$ [m s^{-1}]
u_0	fluid velocity in clearance [m s^{-1}]
$\dot{V}$	inlet flow rate [m^3 s^{-1}]
X	tube length [m]
Z	orifice shape factor.

Greek symbols

α	heat transfer coefficient [W (m^{-2} K^{-1})]
δ	baffle thickness [m]
λ	thermal conductivity [W (K m)$^{-1}$]
v	kinematic viscosity [m^2 s^{-1}]
ψ	tube bundle porosity $\psi = 1 - \pi/(4a)$
ζ	pressure drop coefficient $\zeta = \dfrac{2\Delta P_1}{\rho u^2} \cdot \dfrac{d}{L}$
ζ_0	pressure drop coefficient $\zeta_0 = \dfrac{2\Delta P_2}{\rho u_0^2}$.

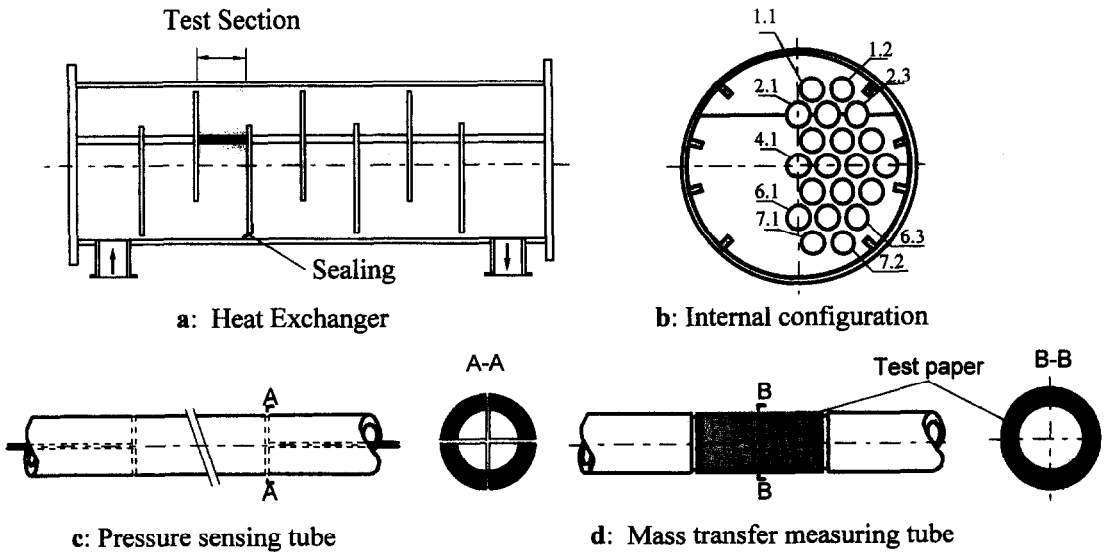

Fig. 1. Construction of the heat exchanger and measuring tubes.

Table 1. Main dimensions and features of the heat exchanger

Item	Dimensions and description	Item	Dimensions and description
Inside diameter of shell	290 mm	Pitch ratio	1.26
Diameter of baffle holed	30.4 mm	Baffle cut	27% of shell inside diameter
Diameter of baffles	286 mm	Number of tube	37
Outside diameter of tubes	30 mm	Baffle thickness	10 mm
Baffle spacing	113 mm	—	—

solubility, it is absorbed quantitatively in the wet filter paper according to local partial concentration differences. After absorption, the following reactions take place:

$$NH_3 + H_2O \rightleftharpoons NH_4^+ + OH^-$$

$$2NH_4OH + MnCl_2 \rightarrow 2NH_4Cl + Mn(OH)_2$$

$$Mn(OH)_2 + H_2O_2 \rightarrow MnO_2\downarrow + 2H_2O.$$

The colour intensity of manganese dioxide corresponds to the locally transferred mass rate.

The local transferred mass is determined by optical measurements. After the experimental run the wet test paper is removed from the measuring tube surface and dried. The dried test paper is located on the cross table of the remission photometer, as shown in Fig. 2. The colour intensity is evaluated and converted to local mass transfer by using a calibration curve. The local heat transfer coefficients are attained from the analog between the mass and heat transfer.

Pressure drop measurements were made within the tube bundle. The plexiglass pressure sensing tubes have eight 1.0 mm tappings [see Fig. 1(c)]. For the measurements of the pressure drop (ΔP_1) in two baffle compartments, the tappings were located under the second and fourth baffles. In order to calculate the leakage rate through the baffle-shell clearance and the baffle-tube clearance, the pressure drop (ΔP_2) in these clearances was also measured. During the experiments, the pressure sensing tube was inserted in the positions of the central tubes of rows (2–7) successively, and the tappings were located just before and after the third baffle.

RESULTS AND DISCUSSION

Local heat transfer

Figure 3(a) shows the photo of the distribution of the local transferred mass on the surface of the tube 1.2, at which the baffle-shell leakage rate is greatest, for $Re = 8000$ with baffle-shell leakage. The corresponding three-dimensional distribution of the local Nusselt number is demonstrated in Fig. 3(b), where X is the tube length in the tested baffle compartment and the line is the circumferential position as shown in this figure. From $X = 0$–10 mm, the local mass and heat transfer distribution in the baffle-tube clearance is presented. Because of the long unsupported span in the window zone, this plexiglass mass transfer measuring tube is in contact with the baffle. It follows that the mass and heat transfer in the baffle-tube clearance is similar to that in a tangent annular orifice. The high local Nusselt numbers at $X = 0$ are due to the thin boundary layer in the annular orifice entrance. From $X = 10$–123 mm, the line 10 with high local heat transfer coefficients corresponds to the stagnation line. The profile of the local Nusselt number along the tube length reveals qualitatively the cross flow velocity distribution in the outlet window zone. The lines 7 and 13 represent the separation of the boundary layer in the front portion of the tube. The contribution of the baffle-shell leakage to the local mass and heat transfer

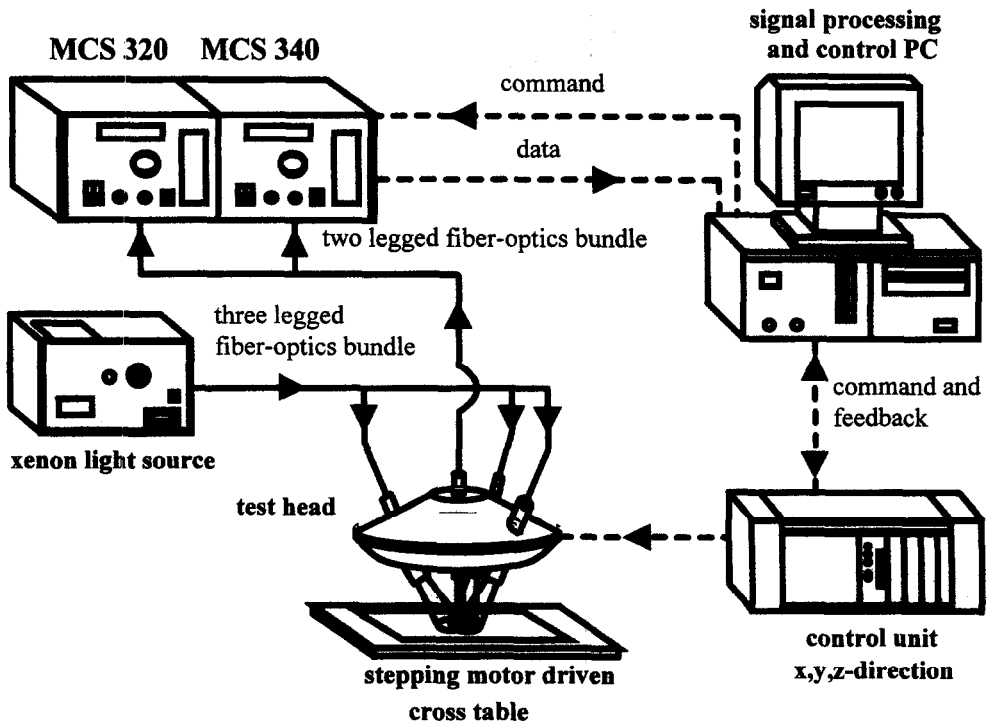

Fig. 2. Remission photometer for quantitative determination of local mass transfer coefficients.

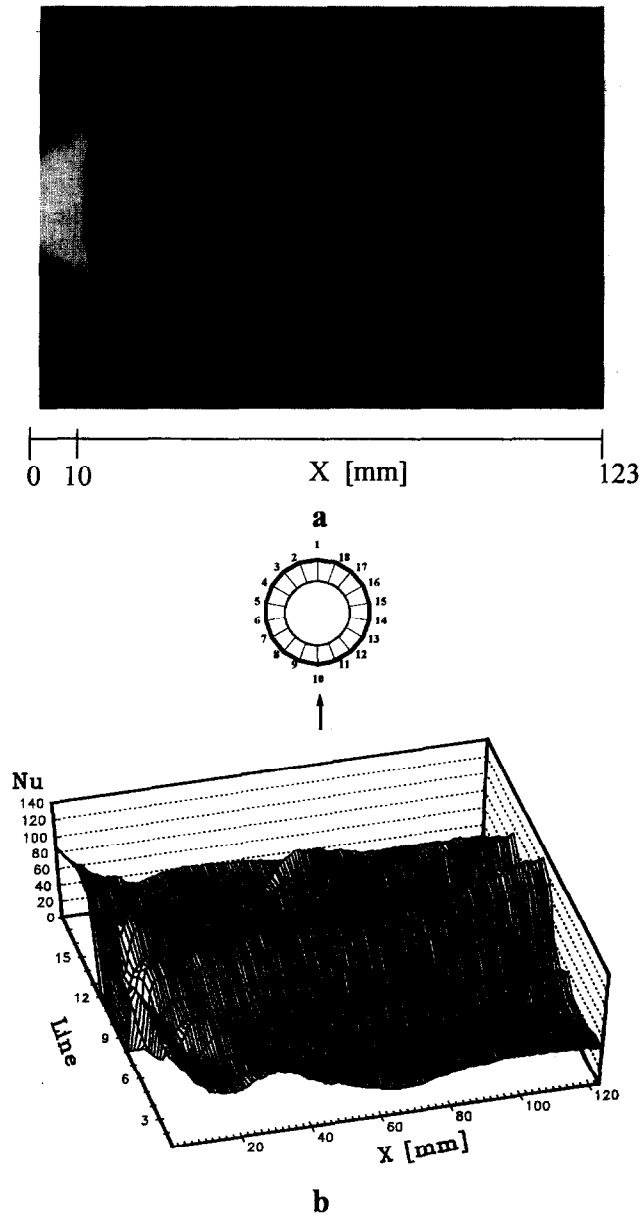

Fig. 3. Visualization and distribution of local mass and heat transfer on the surface of the tube 1.2 for $Re = 8000$ and with baffle-shell leakage.

can be observed from the darker area in Fig. 3(a) as well as its corresponding high local Nusselt numbers by the lines 16 and 17 for $X > 48$ mm in Fig. 3(b).

Integral heat transfer and pressure drop

Figure 4 shows the circumferential distributions of the average Nusselt number of the tube bundle in the tested baffle compartment for $Re = 8000$ without and with baffle-shell leakage, where the per-tube average Nusselt numbers are presented as well. These distributions give a detailed information about the mass and heat transfer in one fully-developed compartment. With the aid of stagnation point at each tube surface, they reveal also the shell-side flow patterns. Because of the dominance of longitudinally directed flow, the local Nusselt numbers in the inlet window zone located at the bottom of this figure are smaller than those in the cross-flow and outlet window zones, while the difference between the cross-flow zone and the outlet window zone is not obvious.

The effect of the baffle-shell leakage on the heat transfer is remarkable. Due to this leakage, the per-tube Nusselt numbers of the external tubes of the tube bundle (e.g. tubes 1.2, 2.3, 3.3 and 4.1, which are in contact with this leakage) are slightly higher than those of the internal tubes, as shown in Fig. 4(b).

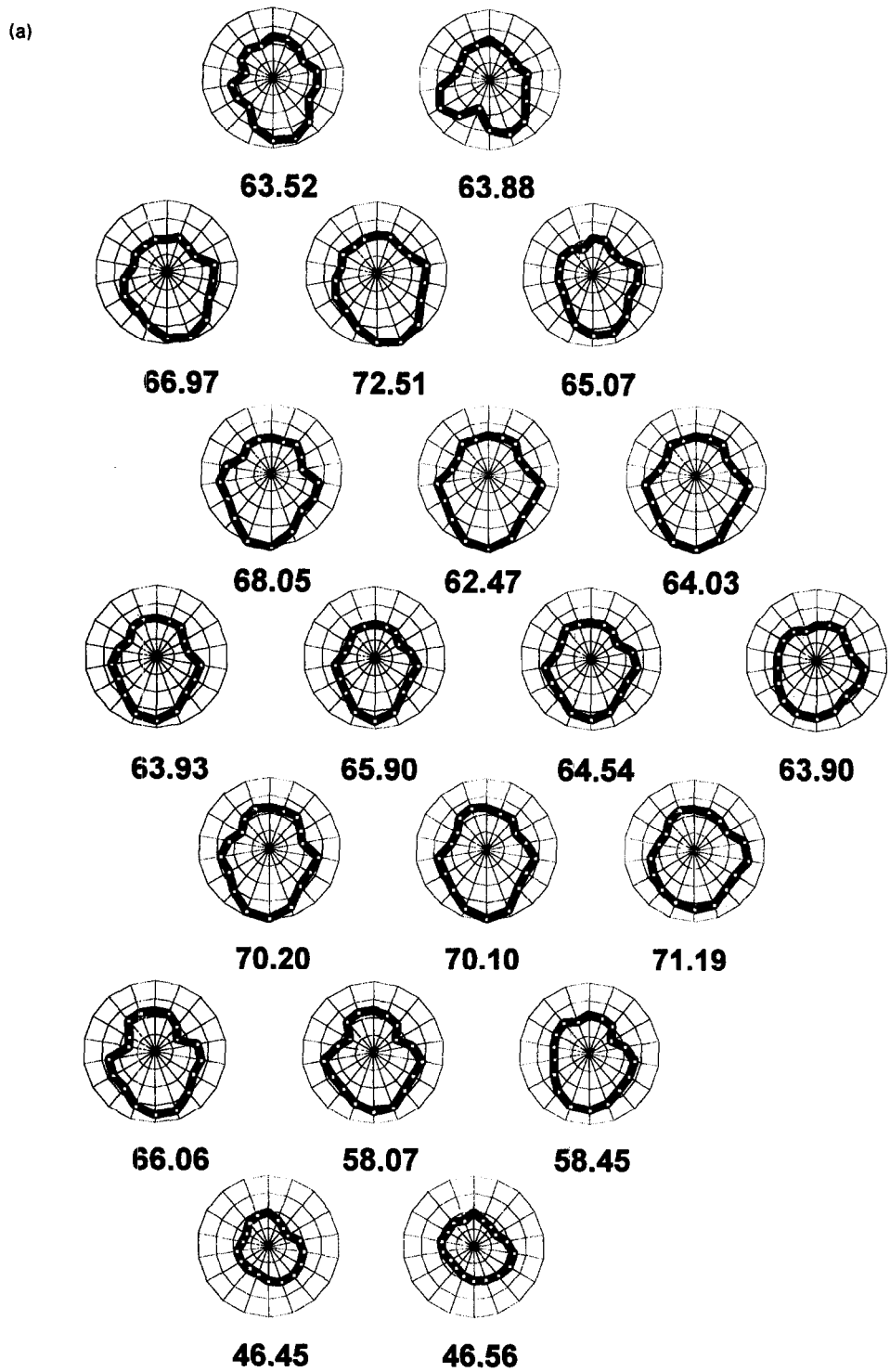

Fig. 4.(a) Circumferential distributions of the local Nusselt number averaged over the tube length for $Re = 8000$ without baffle-shell leakage; (b) circumferential distributions of the local Nusselt number averaged over the tube length for $Re = 8000$ with baffle-shell leakage.

(b)

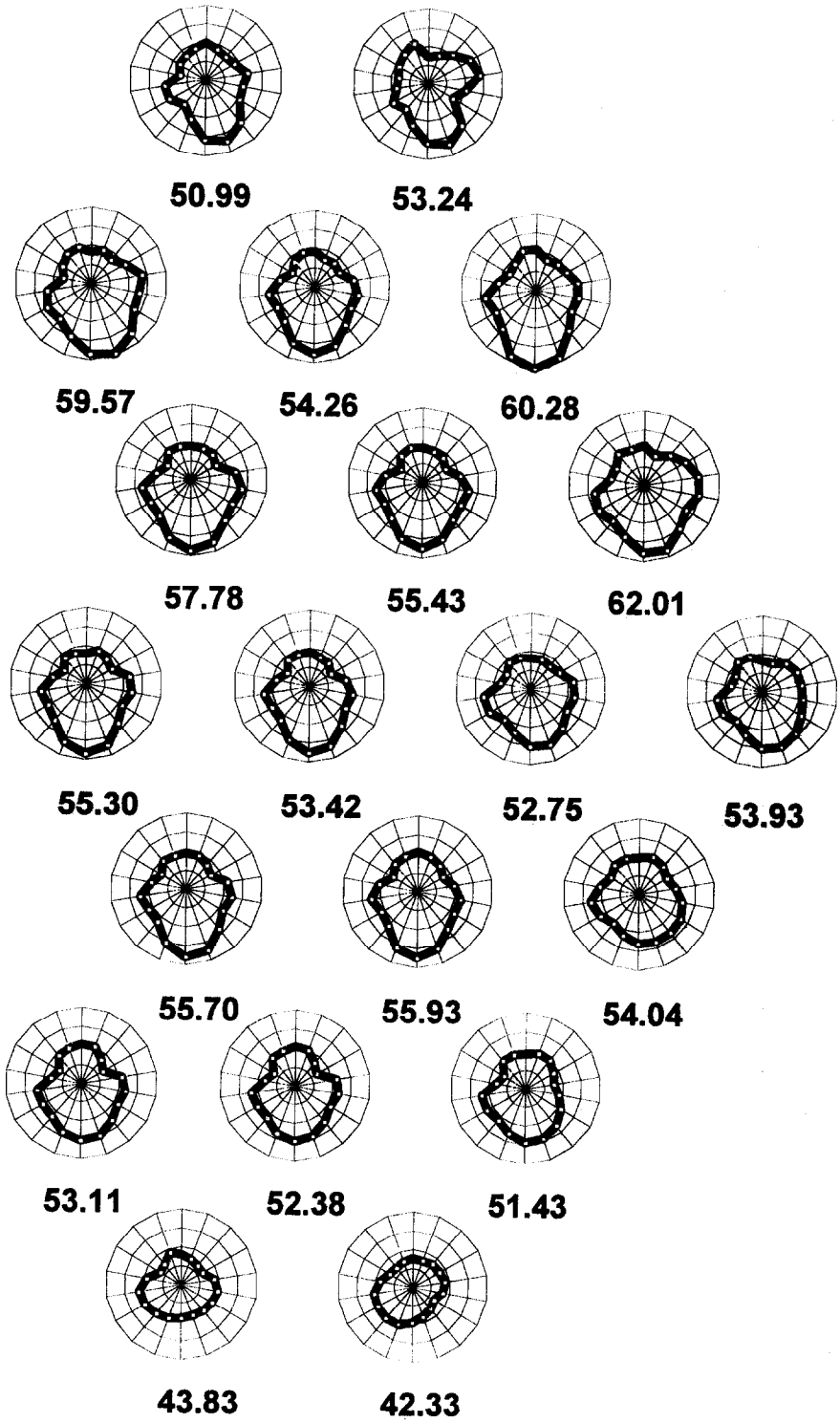

Fig. 4—*continued.*

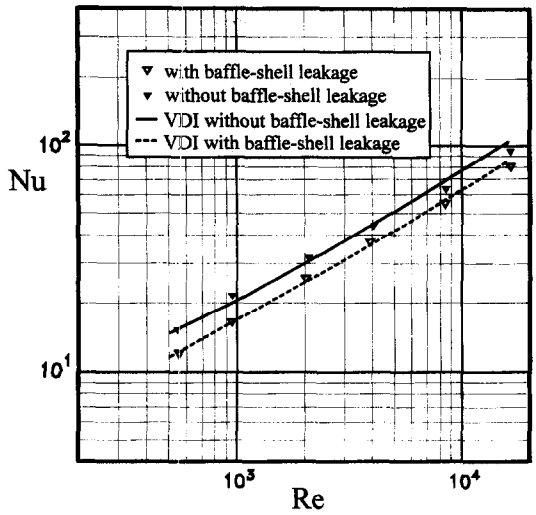

Fig. 5. Per-compartment Nusselt number as function of Reynolds number.

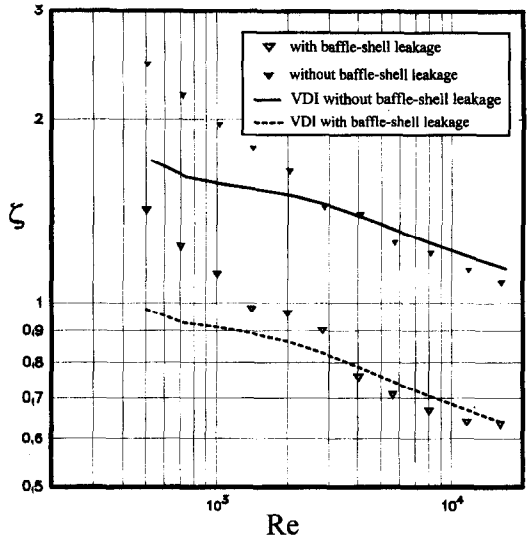

Fig. 6. Pressure drop coefficients in two baffle compartments.

However, the per-compartment average Nusselt number is reduced about 18% by this leakage for $Re = 8000$ (based of the same inlet volume rate).

The per-compartment average Nusselt number is drawn from the local values and given as function of Reynolds number in Fig. 5. Compared to the literature data, Fig. 5 shows a good agreement with the VDI-Wärmeatlas [12]. The baffle-shell leakage reduces the per-compartment average Nusselt number about 21% for $Re = 500$ and 17% for $Re = 16{,}000$.

Figure 6 shows the pressure drop coefficients in two baffle compartments and the calculated values from VDI-Wärmeatlas [13]. The baffle-shell leakage also reduces the shell-side pressure drop greatly, about 74% for $Re = 500$ and 69% for $Re = 16{,}000$. A good agreement between the results of this study and the values from VDI-Wärmeatlas can be observed in Fig. 6 for $Re > 3000$.

Flow distribution

The fluid velocity u_0 through either the baffle-shell clearance or the baffle-tube clearance can be calculated from

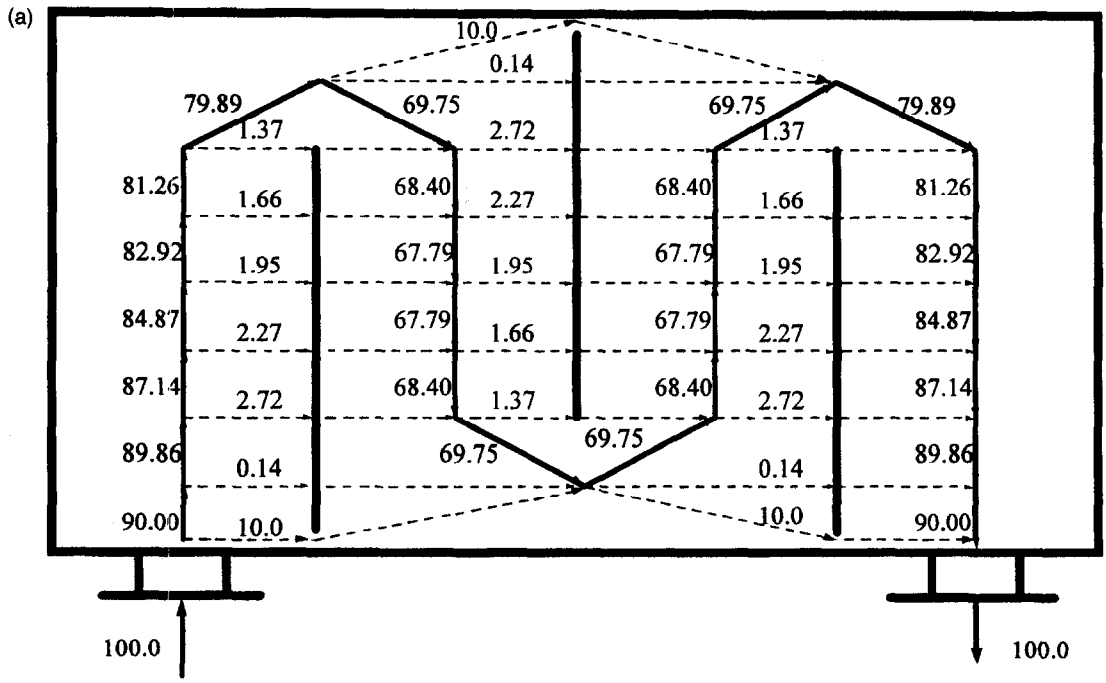

Fig. 7. (a) Shell-side flow distribution for $Re = 8000$ with baffle-shell leakage; (b) shell-side flow distribution for $Re = 8000$ without baffle-shell leakage.

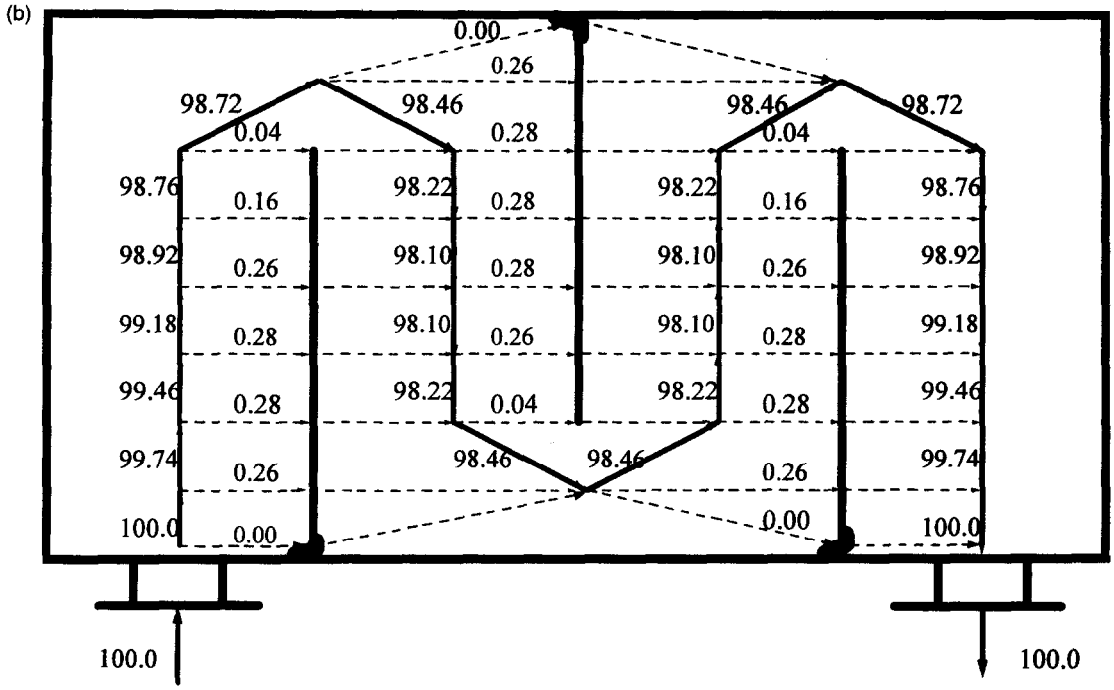

Fig. 7—*continued.*

$$u_0 = \sqrt{\frac{2\Delta P_2}{\rho \zeta_0}} \tag{1}$$

if the pressure drop ΔP_2 due to flow through these clearances and the pressure drop coefficient ζ_0 are known. According to Kukral [7], ζ_0 depends primarily on the orifice Reynolds number Re_0 and the orifice shape factor Z

$$\zeta_0 = f(Re_0, Z) \tag{2}$$

$$Re_0 = w_0(D-d)/\nu \tag{3}$$

$$Z = 2\delta/(D-d) \tag{4}$$

where D and d denote outer and inner diameter of the annular orifices in a plate of thickness δ. Figure 7(a) presents the flow rate of the baffle-shell leakage and the baffle-tube leakage at different positions of the tube rows relative to the volume flow rate at the entrance for $Re = 8000$, while Fig. 7(b) shows only the flow rate of the baffle-tube leakage. The leakage rate through the baffle-tube clearances is much smaller than that through the baffle-shell clearance. In consideration of the high Nusselt number in the baffle-tube clearances as shown in Fig. 3(b), this baffle-tube leakage is positive to the shell-side heat transfer. The baffle-shell leakage can reach up to 20% of the inlet flow rate in this investigated heat exchanger for $Re = 8000$ and is greatest at the roots of the baffles, as shown in Fig. 7(a). This is the reason, why the baffle-shell leakage can strongly influence the shell-side heat transfer and pressure drop.

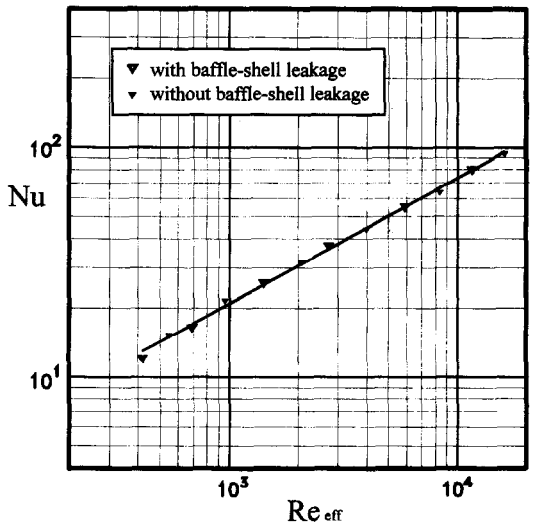

Fig. 8. Per-compartment Nusselt number as function of effective Reynolds number.

Figure 8 shows the per-compartment average Nusselt number as function of the effective Reynolds number Re_{eff}, which is based on the effective main flow rate in the cross-flow zone of a fully developed baffle compartment. The difference in Fig. 5 induced by the baffle-shell leakage then disappears. The Nusselt numbers with and without baffle-shell leakage can be expressed as a function of the effective Reynolds number.

$$Nu = 0.566 Re_{\text{eff}}^{0.543} Pr^{0.33}. \tag{5}$$

This shows a good agreement between the results of the heat transfer experiments and the calculated flow distribution. It proves that the correlation suggested by Kukral can be used to accurately predict the shell-side flow distribution.

CONCLUSIONS

The effects of the leakage on pressure drop and local heat transfer in shell-and-tube heat exchangers has been experimentally investigated. The baffle-shell leakage has slight contribution to the local heat transfer at the surfaces of the external tubes of the tube bundle, but reduces greatly the per-compartment average heat transfer, for $Re = 500$ up to 21% and for $Re = 16{,}000$ up to 17%. The reduction of the pressure drop coefficient due to this leakage reaches up to 74% for $Re = 500$, and up to 69% for $Re = 16{,}000$. The baffle-tube leakage is positive for the improvement of the heat transfer and for the reduction of the pressure drop. Using the correlation suggested by Kukral, the shell-side flow distribution can be accurately predicted from the pressure drop in the clearances. Based on the effective flow velocity in the cross-flow zone of the fully developed baffle compartment, the shell-side heat transfer can be expressed as $Nu = 0.566\ Re_{\text{eff}}^{0.543} Pr^{0.33}$.

REFERENCES

1. Bell, K. J., Final report of the cooperative research program on shell and tube heat exchangers. University of Delaware Engineering experimental Station, Bulletin no. 5, 1963.
2. Bergelin, O. P., Bell, K. J. and Leighton, M. D., Heat transfer and fluid friction during flow across banks of tubes—VI the effect of internal leakages within segmentally baffled exchangers. *Transactions of the ASME*, 1958 53–60.
3. Tinker, T., Shell side characteristics of shell and tube heat exchanger, Part I, II, III. *General Discussion on Heat Transfer*. The Institution of Mechanical Engineers, London, 1951, pp. 89–116.
4. Palen, J. W. and Taborek, J., Solution of shell side flow pressure drop and heat transfer by stream analysis method. *Chemical Engineering Progress Symposium Series*, 1969, **92**, 53–63
5. Gaddis, E. S. and Schlünder E. U., Einfluß der Leckströmung auf Temperatureverlauf und übertragbare Wärmemenge in Röhrenkesselapparaten mit Umlenkblechen. *Verfahrenstechnik*, 1976, **10**, 191–194.
6. Roetzel, W. and Xuan, Y., Dispersion model for divided-flow heat exchanger. *Proceedings of EUROTHERN Seminar No.* 18, *Hamburg*, 1991, pp. 98–110.
7. Kukral, R. and Stephan, K., The effect of internal leakage on steady-state and transient behaviour of shell-and-tube heat exchangers. *Proceedings of* 10*th International Heat Transfer Conference*, Brighton, U.K. 1994, pp. 393–398.
8. Kottke, V., Blenke, H. and Schmidt, K. G., Eine chemische farbreaktion zur Messung örtlicher Stoffübertragung und Sichtbarmachung von Strömungsvorgängen. *Wärme- und Stoffübertragung*, 1977, **10**, 9–21.
9. Kottke, V., A chemical method for flow visualization and determination of local mass transfer, flow visualization II. *Proceedings of the Second International Symposium on Flow Visualization*, Bochum, Germany, 1980, pp. 657–662.
10. Kottke, V., Blenke, H. and Schmidt, K. G., Messung und Berechnung des örtlichen und mittleren Stoffübergangs an stumpf angeströmten Kreisscheiben bei unterschiedlicher Turbulenz. *Wärme- und Stoffübertragung*, 1977, **10**, 89–105.
11. Kottke, V. and Schmidt, K. G., Measuring techniques for determination of local mass heat transfer in industrial scale. *Proceedings XV JCHMT Symposium Heat and Mass Transfer Measurements*, Washington, 1985, pp. 1–11.
12. Gaddis, E. S. and Gnielinski, V., Wärmeübertragung im Außenraum von Rohrbündel-Wärmeübertragern mit Umlenkblechen. In *VDI-Wärmeatlas*, 6. Aufl. VDI-Verlag, Düsseldorf, 1991, pp. Gg 1–6.
13. Gaddis, E. S., Druckverlust im Auenraum von Rohrbündel-Wärmeübertragern mit und ohne Einbauten. In *VDI-Wärmeatlas*, 6. Aufl. VDI-Verlag, Düsseldorf, 1991, pp. Lm 1–10.